Journal of Zhejiang University-SCIENCE A (Applied Physics & Engineering)
ISSN 1673-565X (Print); ISSN 1862-1775 (Online)
www.jzus.zju.edu.cn; www.springerlink.com
E-mail: jzus@zju.edu.cn

Discrete element analysis of a cross-river tunnel under random vibration levels induced by trains operating during the flood season*

Zhi-hua ZHANG[†1], Xie-dong ZHANG[1], Yao TANG[2], Yi-fei CUI[3]

[1]*School of Transportation, Wuhan University of Technology, Wuhan 430063, China*

[2]*Department of Civil and Environmental Engineering, University of Alberta, Edmonton, Alberta T6G 2R3, Canada*

[3]*Department of Civil and Environmental Engineering, Hong Kong University of Science and Technology, Hong Kong, China*

[†]E-mail: zzh@whut.edu.cn

Received Jan. 4, 2017; Revision accepted July 11, 2017; Crosschecked Apr. 11, 2018

Abstract: Floods result in many problems, which may include damage to cross-river tunnels. The cross-river tunnel, as a new style of transportation, deserves a large amount of attention. In this paper, a large-scale cross-river tunnel model is proposed based on discrete element method (DEM). Micro parameters used in the model are calibrated by proposing a triaxial numerical model. Different in situ strata, high water pressures of normal flood-water levels and random vibration levels induced by running trains are taken into account to evaluate the dynamic characteristics of a high-stress tunnel in deformation and stress analysis. The results show that the upper half of the tunnel, including the concrete lining and the surroundings, is at higher risk than the lower half. Vibration waves transferring into the surroundings undergo an amplification process. The particles of the surroundings at the vault of the tunnel separate and move downward and then reassemble during the dynamic vibrations. The vibration levels, represented by particle accelerations, are lower under flood conditions than those under normal conditions. As train speed increases, the acceleration of the track and particles in the foundation increases, accompanied by a decrease in deformation.

Key words: Discrete element method (DEM); Cross-river tunnel; Water pressure; Metro train operation; Random vibration level; Acceleration

https://doi.org/10.1631/jzus.A1700002 **CLC number:** U25

1 Introduction

The rapid development of engineering technology has played an important role in the development of underground spaces. The numbers of subways, multilayer underground parking structures, cross-river tunnels, and undersea tunnels have grown significantly over recent decades. In particular, cross-river tunnels have been constructed in developed cities, such as Shanghai, Guangzhou, and Wuhan in China, and transport large numbers of passengers. Thus, an increasing number of cities are paying attention to cross-river tunnels.

Subway tunnels are built in urban areas to save space on the land surface for living and for environmental reasons. Trains running underground induce high vibration and noises in the ground and in nearby buildings. To attempt to track the vibrations and noises induced by running trains in shield channels, field experiments and surveys have been conducted (Ling et al., 2010; Abul-Husn et al., 2013; Kouroussis, 2013; Connolly et al., 2015a, 2015b; Zhai et al., 2015). Unlike the common train-induced vibrations in a residential area, vibrations in the surroundings of a cross-river tunnel are not the only indicator to be taken into account. Since these trains are operating in

* Project supported by the Fundamental Research Funds for the Central Universities of China (No. 2017-YB-014) and the National Natural Science Foundation of China (No. 51408450)

ORCID: Zhi-hua ZHANG, https://orcid.org/0000-0003-1583-9311

© Zhejiang University and Springer-Verlag GmbH Germany, part of Springer Nature 2018

a deep underground environment, the stability of the concrete lining, the permeability of the surroundings and lining, and the high water-pressure distribution around the tunnel should be considered as well. High water pressure may lead to the collapse of the concrete lining. Therefore, the situation of a tunnel under water is more complicated than that of a tunnel in an urban area.

The reinforced lining used in a cross-river tunnel should be specifically designed with high strength and low permeability. Voit and Zimmermann (2015) analyzed the characteristics of aggregates and different cement types in the concrete lining of an underground tunnel in a soft soil situation subjected to high water pressure. Gao et al. (2012) studied the dynamic characteristics and failure mechanism of a cross-river tunnel using the 3D dynamic finite-difference method. The failure mechanism included several aspects, such as a damage zone in the surrounding rock and soil, cracking of the concrete lining, and permeability deterioration. After the lining cracks, the permeability of the lining will drastically increase (Aldea et al., 1999; Picandet et al., 2009) and the high water pressure will transform the outside of the lining (Zhou et al., 2015). Since the hydraulic coefficient of the concrete lining is about 1×10^{-9} m/s (Min et al., 2010) and the maintenance duration is relatively short, the effect of seepage on tunnel-face stability is expected to be small before the cracking of the concrete lining. Thus, the effect of seepage is neglected in this study.

Southern China has a rainy season during which the Yangtze River is prone to flooding. During this period, the water level will increase by 10 m or more. Therefore, the design requirements of the cross-river tunnel should take the flood period into account. The stress, deformation, and vibrations induced by running trains in the tunnel during the flood period should be analyzed and compared with those under normal water pressure (NWP) during the non-rainy season. However, little has been published on this subject.

In this paper, the discrete element method (DEM) of particle flow code (PFC) is used for numerical simulation. DEM has unique advantages for modeling materials in discontinuum because the contact force chains and cracks can be obtained and are independent of the results from numerical mesh design. A cross-river tunnel model is established based on the Metro Line 2 cross-river tunnel project in Wuhan. Different strata and water pressures of normal and flood water levels are considered. Random vibration levels induced by running trains have been proposed in studies by Colaço et al. (2015) and Connolly et al. (2015b). The influence of random vibration levels on the concrete lining and the surroundings has been studied. The purpose of this paper is to analyze the impact of random vibration levels generated by running trains at different speeds under NWP and flood water pressure (FWP). We use a novel approach based on the DEM to simulate train operations in the cross-river tunnel with various water pressures. The effects on concrete stability and the characteristics of the surroundings of vibrations induced by running trains are analyzed. The results provide a deeper understanding of how cross-river tunnel behavior is affected by metro train operations during the flood season.

2 Project overview

2.1 Project site

The Metro Line 2 is one of the largest passenger transportation lines in the Wuhan Metro Transit system. The starting station is Jinyin Tan Station, which is located in Hankou District; the line crosses some main areas, such as Hankou Railway Station and two prosperous squares, and passes through a 3100 m-long cross-river tunnel running from northwest of the river at Jianghan Road Station to southeast of the river at Jiyu Bridge Station (Fig. 1). The single tunnel containing a single line was excavated using a shield-driving method and has a diameter of 6.52 m.

2.2 Geological background

Fig. 2 depicts a partial view of the main geological strata of the Yangtze River. The cross-river tunnel passes mainly through sand layers, including mud rock, fine sand, and coarse sand, with high permeability and low clay content (Zhang et al., 2013; Xiong, 2014; Min et al., 2015). The subsurface soil under the river consists of silty clay, coarse sand, and mud rock. To determine the relevant parameters, samples of each layer were taken into the lab to conduct consolidated undrained triaxial tests. The

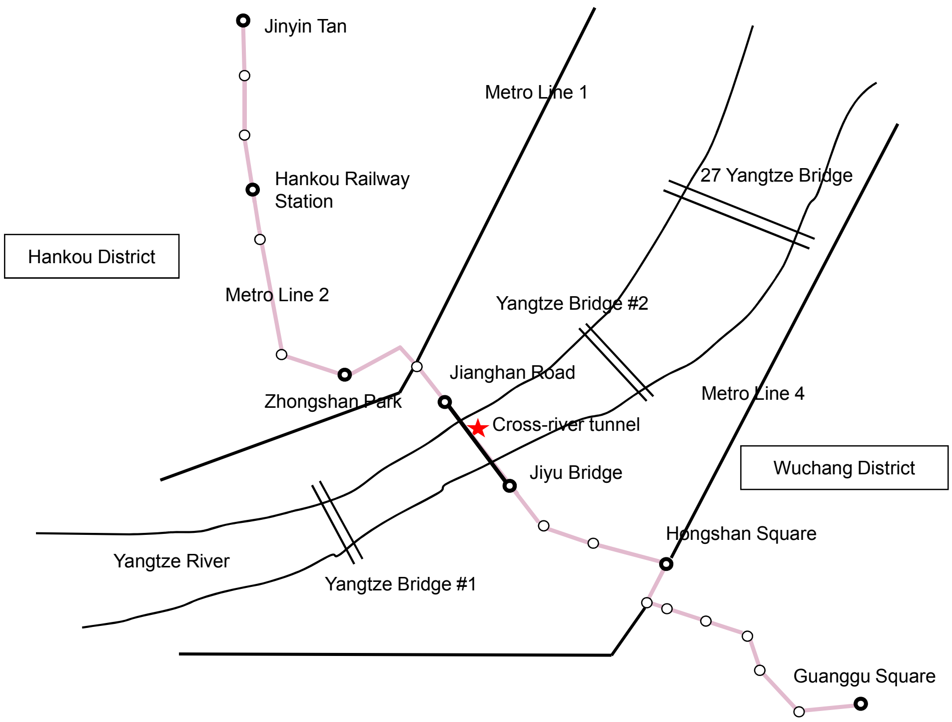

Fig. 1 Location of Wuhan Metro Line 2 and cross-river tunnel

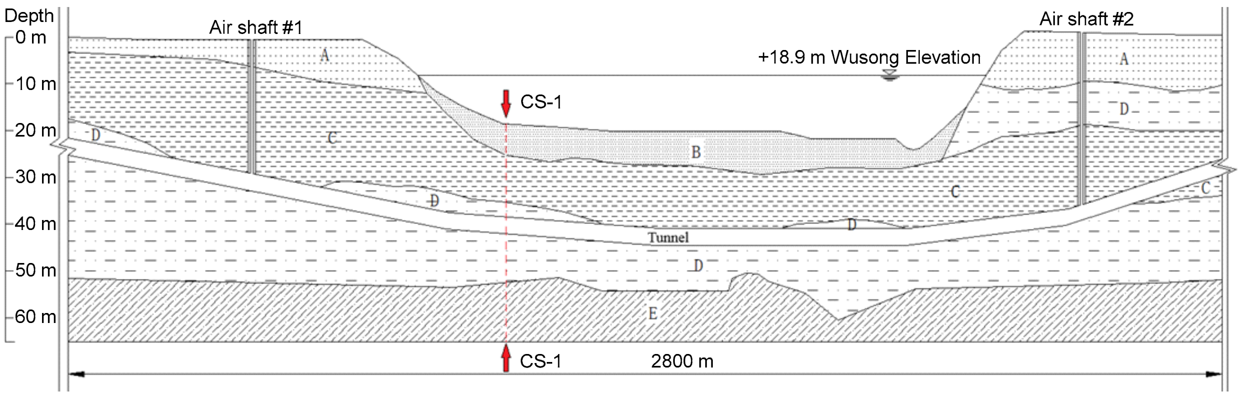

Fig. 2 Location of the tunnel (CS-1) and soil profile

A: fine sand (containing some clay); B: silty clay; C: coarse sand (containing some gravel); D: coarse sand (containing some cobble); E: bedrock (mud rock); CS-1: cross-sectional surface (for numerical analysis)

details of the triaxial tests in the laboratory are described in Section 4.1.

3 Discrete element method

In this study, the dynamic characteristics of the concrete lining and the surroundings affected by random vibrations in the cross-river tunnel under normal and flood water levels under high-stress conditions are considered. The following assumptions are made:

1. The seepage in the strata is neglected due to the waterproof property of the concrete lining. In the numerical simulation, the concrete lining proposed in the model is assembled with a highly cohesive bond that has low permeability. The total water pressure calculated according to the depth of the water above the tunnel roof acts on the top of the model. Therefore, the water pressure was taken into account in the boundary conditions, and the seepage flow during the dynamic process was neglected.

2. The buoyancy force acting on the particles is considered in the model. To determine the buoyancy effect on the whole model, the buoyancy force of each particle is calculated as $F_p=\rho g V_p$, where ρ and V_p are the density and volume of the particle, respectively, and g is the gravitational acceleration. The buoyance force is then applied to each of the particles in the opposite direction to the gravitational force.

3. It is assumed that the initial stress of the whole layer is uniform before the excavation of the tunnel. A consolidation process has been executed with the value of the associated water pressure before excavation; the details of the excavation process are given in Section 4.5.

4. The water surface of the Yangtze River is assumed to be flat, without any fluctuating wave movements.

Although the present model is not an exact solution, it is useful for assessing the influence of random vibrations on concrete stability and the creep of the surroundings for the cross-river tunnel in the flood season. The complex anisotropic properties of soil, especially the hydrostatic properties, are critical for predicting potential risks in the construction and maintenance of a cross-river tunnel.

The DEM has a number of advantages in numerical simulations: it can be applied to material of any viscoelasticity or plasticity and does not require a prescribed initial micro-crack fabric. Therefore, this method is widely used for modeling crack growth. By default, all contacts are assigned the linear model by associating a spring and dashpot with each contact (Potyondy and Cundall, 2004). The linear model includes several contact-bond behaviors, such as unbonded interaction in the rail-sleeper, sleeper-foundation and concrete lining the surroundings, and parallel and contact bonded interaction of particles in the concrete lining and surrounding materials, respectively. For the elastic-plastic materials used in this model, a number of Kelvin and Maxwell models of the spring and dashpot (Itasca, 2008) connected in series in the normal and shear directions are used to simulate the creep mechanism. A schematic representation of the Kelvin and Maxwell model is shown in Fig. 3.

The total displacement of the Kelvin and Maxwell model, u, is the sum of the displacements of the Kelvin section, u_k, and those of the Maxwell sections, u_m, which includes u_{mk} and $u_{m\eta}$. Their relationship is illustrated as

$$u=u_k+u_{mk}+u_{m\eta}. \tag{1}$$

The first and second derivatives of Eq. (1) are given in the following equations:

$$\dot{u}=\dot{u}_k+\dot{u}_{mk}+\dot{u}_{m\eta}, \tag{2}$$

$$\ddot{u}=\ddot{u}_k+\ddot{u}_{mk}+\ddot{u}_{m\eta}. \tag{3}$$

The contact force, f, using the Kelvin and Maxwell sections, is calculated by

$$f=\begin{cases}\pm K_k u_k \pm \eta_k \dot{u}_k, \\ \pm K_m u_{mk}, \\ \pm \eta_m \dot{u}_m, \end{cases} \tag{4}$$

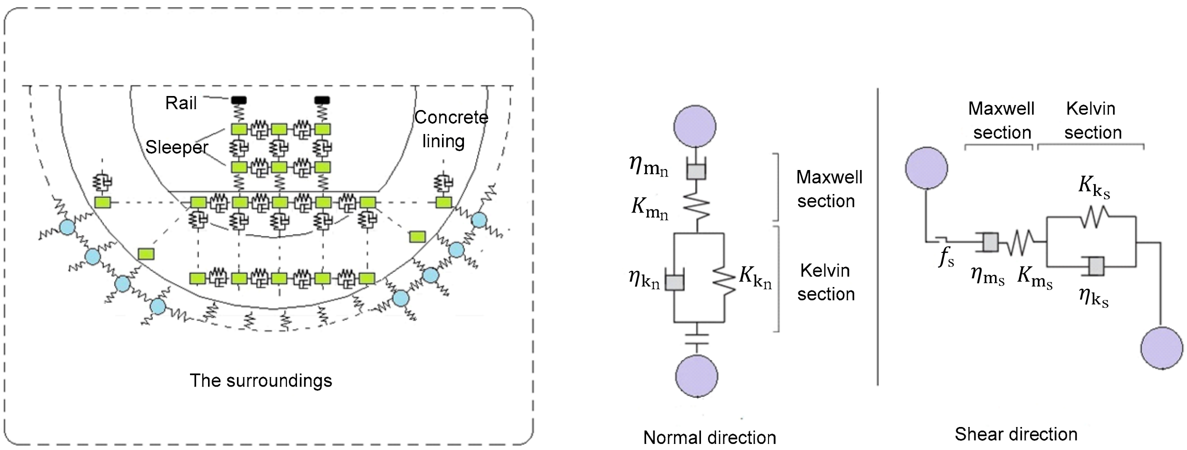

Fig. 3 Coupled contact model of a cross-river tunnel: Kelvin and Maxwell model
Subscripts n and s represent normal and shear directions, respectively

where K_k and η_k are the stiffness and viscosity for Kelvin section, and K_m and η_m are the stiffness and viscosity for Maxwell section, respectively.

Substituting Eq. (4) and its first derivative into Eqs. (2) and (3), the second-order differential equation for the contact force f is given by

$$f = a_1\dot{f} + a_2\ddot{f} = b_1\dot{u} + b_2\ddot{u}, \tag{5}$$

where $a_1 = \dfrac{\eta_k}{K_k} + \eta_m\left(\dfrac{1}{K_k} + \dfrac{1}{K_m}\right)$, $a_2 = \dfrac{\eta_k\eta_m}{K_k K_m}$, $b_1 = \pm\eta_m$, and $b_2 = \pm\dfrac{\eta_k\eta_m}{K_k}$.

The Laplace transform of Eq. (5) is given by Eq. (6) under the initial conditions $u = \dot{u} = 0$ and $f = \dot{f} = 0$.

$$(1 + a_1 s + a_2 s^2)F(s) = (b_1 s + b_2 s^2)U(s), \tag{6}$$

where s is the variable deduced by the Laplace transform, $U(s) = L\left[u(t)\right]$, and $F(s) = L\left[f(t)\right]$. Here, the Laplace transform of a generic function $u(t)$ is

$$L\left[u(t)\right] = \int_0^\infty \mathrm{e}^{-st}u(t)\mathrm{d}t. \tag{7}$$

Therefore, the analytical solution in the time domain for unit displacement $u(t)=1$ is given by

$$f(t) = A_1\,\mathrm{e}^{z_1 t} + A_2\,\mathrm{e}^{z_2 t}, \tag{8}$$

where z_1 and z_2 are the roots of the quadratic equation $a_2s^2+a_1s+1=0$, $A_1 = \dfrac{b_2 z_1 + b_1}{a_2(z_1 - z_2)}$, and $A_2 = \dfrac{b_2 z_2 + b_1}{a_2(z_2 - z_1)}$. Based on the equations given above, the stress field of the tunnel is calculated.

4 Cross-river tunnel model

Compared with 3D DEM, a 2D model is used for plain strain calculation, as well as for improving the calculation speed (Wang and Gutierrez, 2010; Liu and Koyi, 2013). With the assumption of isotropic subsurface soils with finite thickness along the Yangtze River, the numerical model can be constructed in the direction of the tunneling of the shield tunnel machine. Vibrations induced by a running train can be easily simulated on the rails. Moreover, the main deformation of the tunnel, if it exists, is along the direction of normal stress; the deformation in the longitudinal direction may be irrelevant. Therefore, it is necessary and feasible to construct the cross-river tunnel model to analyze the complicated situation with high water pressure using a 2D numerical approach.

4.1 Triaxial tests in the laboratory

In the experimental study, conventional triaxial tests ($\sigma_2=\sigma_3$) were carried out on silty clay materials, which can be considered as granular materials and are easily simulated by the DEM. The experimental specimens were assembled into a cylindrical shape with a diameter of 50 mm and a height of 125 mm. The density and void ratio were controlled to be the same as those in situ. Confining stresses were imposed on the specimen with different values of 125 kPa and 350 kPa. Each specimen was prepared using the same procedures for consolidated undrained triaxial tests as used by others (Wu et al., 2017).

The test specimen of silty clay and the test apparatus are shown in Fig. 4. The test results of deviator stress versus axial strain are illustrated in Section 4.2. The associated macro parameters of silty clay properties were determined based on the laboratory results (Table 1).

For fine sand and coarse sand, triaxial tests were conducted in the laboratory. The macro parameters are listed in Table 1. The detailed procedures and the results of the triaxial tests can be found in (Lu et al., 2017).

(a) (b)

Fig. 4 Triaxial tests in the laboratory
(a) Experimental specimen; (b) Triaxial test apparatus

Table 1 Basic parameters of each stratum in the cross-river tunnel of Wuhan Metro Line 2

Layer	Soil	γ (kN/m^3)	ω (%)	e	c (kPa)	φ (°)	E_s (MPa)
A	Fine sand	20.5	15.0	0.42	2.0	38.0	24.50
B	Silty clay	16.7	49.5	1.40	14.0	10.5	2.17
C	Coarse sand (containing some gravel)	20.1	16.1	0.44	5.4	42.0	35.40
D	Coarse sand (containing some cobble)	20.7	18.0	0.51	6.2	40.0	38.10

γ: total unit weight; ω: moisture content; e: void ratio; c: cohesion; φ: angle of internal friction; E_s: bulk modulus

4.2 Micro-parameter calibration for DEM simulation

The micro-properties of the materials should be calibrated before the model is used to simulate metro train operation. In this calibration procedure, the relationships between the micro parameters and the macro-property responses can be established by adjusting the input micro parameters in a series of triaxial test simulations. The micro parameters of each stratum can be determined by matching the macro responses of each stratum based on the test results in the laboratory.

For coarse sand containing some gravel and cobble represented by layers C and D, respectively, the micro parameter calibrations had been conducted by Lu et al. (2017) from triaxial tests using DEM in numerical simulation. In their model, the minimum size of generated particles was set to 5 mm, which was larger than the original minimum size of 0.075 mm. In our present model, the radii of particles was determined to be 0.06–0.1 m in the large model with a size of 15 m×30 m (width×height) to improve calculation efficiency. Referring to Gu et al. (2017), the ratio of sample size to the mean particle size should be larger than 11.5 to avoid possible scale effects.

For silty clay, triaxial tests were conducted to determine the constitutive relation interpreted by the Mohr-Coulomb model. The Young's modulus and cohesive bond obtained in the laboratory can be directly applied in triaxial simulations, whereas the other uncertain micro parameters, such as stiffness, stiffness ratio, and friction coefficient, should be calibrated from a series of simulations.

Numerical packing with a diameter of 20 mm and a height of 50 mm, which were 0.4 times of the experimental specimens, was conducted with 37990 particles. The radii of the particles (ranging from 0.01 mm to 0.85 mm) used in the DEM were obtained from the particle distributions of samples in the laboratory. The aim of using a numerical specimen with smaller size and particle radius was to control the number of particles generated to facilitate efficient calculation. Particle-size distribution curves of the samples used in the laboratory and DEM are shown in Fig. 5. The assembled particles and the numerical walls are shown in Fig. 6. Soft rubber material was used in the experimental test as the confining wall because the stiffness of the numerical confining wall (wall 7) should be smaller than that of the top and bottom walls (e.g. wall 3 and wall 4, respectively) in the DEM. By convention, the stiffness of the confining wall is 0.1 times of the loading plate.

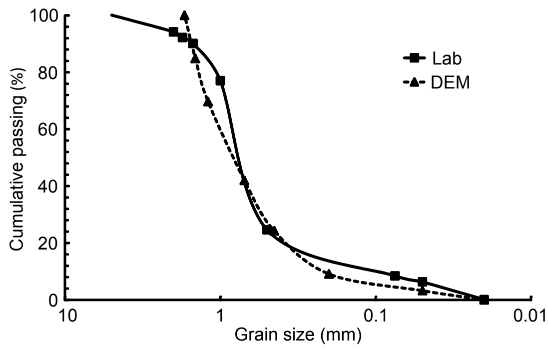

Fig. 5 A comparison of the particle size distribution of the silty clay determined using the DEM simulation and laboratory tests

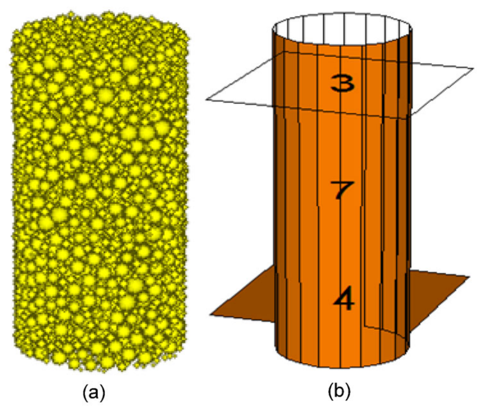

Fig. 6 Particle assembly in triaxial numerical tests
(a) Particle packing; (b) Numerical walls

As depicted in Fig. 7, near perfect matching between numerical tests and laboratory tests was obtained after the uncertain micro parameters of silty clay were adjusted. The micro parameters of each layer used in the discrete element analysis are listed in Table 2.

4.3 Rail modeling

Rail-structure maintenance depends on the mechanical behavior under the influence of dynamic loads. The simplest representation of a continuous linear foundation is the Winkler model (Zhou et al., 2015). Other scholars considered the shortcomings of the Winker model and took the interaction between the ties into account (Nielsen et al., 2003). The material of the rails, in reality, is steel metal, which is unchangeable in the short term. However, the tracks will deform eventually, with the timing and extent of the deformation dependent on the specific geology of the location. According to previous study (Dinis Ferreira, 2010), there are several types of deterioration of the tracks based on the source of damage, resulting in the need for different failure models. In the cross-river tunnel model, rails are modeled as large-sized particles of high stiffness, represented by steel balls of diameter 0.10 m. Therefore, the dynamic load caused by the running train acts on the rail simultaneously. The micro parameters of rail particles are listed in Table 4 (p.355).

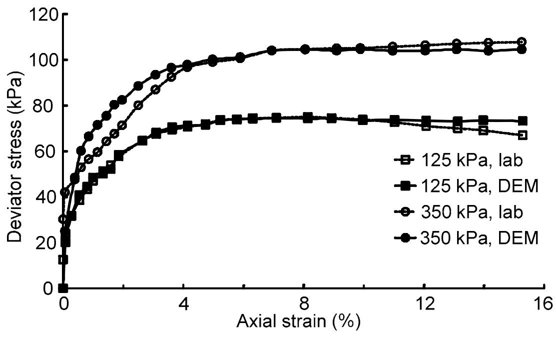

Fig. 7 A comparison of deviator stress versus axial strain between DEM and laboratory results

4.4 Sleeper modeling

The sleeper, as the first apparatus under the rail, can disperse most of the random vibrations to the concrete lining uniformly. Concrete materials were used instead of wood for the sleeper after cohesiveness and stiffness were taken into account. Non-ballast track has been used for metro railways, now that the concrete sleeper connects to the concrete foundation with many fasteners. In the cross-river tunnel model, the deformation of the sleeper can be neglected due to its high stiffness in ideal conditions. The sleeper consists of continuous particles that contact one another according to the expansion command (Fig. 10) (p.356). The size of the sleeper is 2.5 m× 0.25 m (width×height), and the micro parameters of the sleeper are listed in Table 4. The Kelvin-Voigt model (spring-dashpot in parallel) (Fryba, 1999) is regarded as a contact model for a sleeper. In this model, a spring and a dashpot at each contact represent the stiffness and bond, respectively (Fig. 3). The forces are calculated from the stiffness, viscosity, and displacement of the Kelvin-Voigt section, as shown by

$$f = \pm K_{\mathrm{k}} u_{\mathrm{k}} \pm \eta_{\mathrm{k}} \dot{u}_{\mathrm{k}}. \tag{9}$$

By using a central-difference approximation of the finite-difference scheme for the time derivative and taking the average values for u_{k} and f, we obtain

$$\frac{u_{\mathrm{k}}^{t+1} - u_{\mathrm{k}}^{t}}{\Delta t} = \frac{1}{C_{\mathrm{k}}}\left[-\frac{K_{\mathrm{k}}(u_{\mathrm{k}}^{t+1} + u_{\mathrm{k}}^{t})}{2} \pm \frac{f^{t+1} + f^{t}}{2}\right], \tag{10}$$

where C_{k} represents the viscosity of dashpot in the Kelvin model.

The contact force f^{t+1} can be calculated from known values of u_{k}^{t+1}, u_{k}^{t}, and f^{t}. The contact

Table 2 Parameters of each layer used in discrete element analysis

Soil	ρ (kg/m^3)	μ	k_{n} (N/m)	k_{s} (N/m)	n_{bond} (Pa)	s_{bond} (Pa)
Silty clay	1700	0.185	2.17×10^6	2.17×10^6	1.40×10^4	1.40×10^4
Coarse sand (layer C)	2050	0.9	3.54×10^7	3.54×10^7	–	–
Coarse sand (layer D)	2110	0.84	3.80×10^7	3.80×10^7	–	–

ρ: density; μ: friction coefficient; k_{n}: normal stiffness of particles; k_{s}: shear stiffness of particles; n_{bond}: normal cohesive strength of each contact; s_{bond}: shear cohesive strength of each contact between the track and concrete sleeper is complex. Since an additional impact load acts on the upper sleeper, there is only one spring interacting with it (Fig. 3).

4.5 Excavation process

Ji et al. (2013) conducted scanning electron-microscopy and tunnel acoustic-detection tests to analyze the micro-macro mechanical responses of the surrounding rock of tunnels excavated by a tunnel-boring machine and the drill-blasting method. To minimize the disturbance to the surroundings due to excavation, the tunnel-excavation radius should be small at first and then enlarged to the final value of 3.26 m. After the deletion of tunnel particles, smaller particles are generated in the tunnel hole with concrete lining properties of C60; the micro parameters are listed in Table 4. Hereafter, specific particles in the circular tunnel of a 2.75 m radius are deleted, leaving a 50 cm thick annulus as the final lining material. The thickness of the lining in the tunnel model is the same as that in the project. The construction stages of excavation are defined as follows:

Step 1: After model consolidation, particle deletion with increasing radius of the tunnel is executed.

Step 2: A circular wall (casing) without thickness is used for preparing particle generation in the tunnel.

Step 3: Installation of lining particles occurs with lining properties in the area where the particles were deleted. As the particles eliminate the overlaps, the circular wall generated in step 2 is used to prevent them from disturbing the surrounding particles.

Step 4: After the circular wall is deleted, the excavation process is activated with a radius of 0 m for r_0, where r_0 is the radius of tunnel.

The numerical process of constructing the concrete lining is shown in Fig. 8.

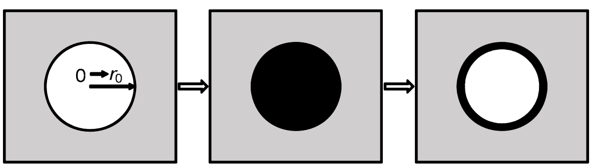

Fig. 8 Numerical process of constructing the concrete lining

4.6 Random vibration levels

In reality, vibrations generated by a train in motion are not simply cyclic, but are random (e.g. not cyclic but irregular). It is necessary to consider the complicated mechanisms of the railway track system, including rails, sleepers, concrete lining, and the surroundings. Random vibration levels induced by a running train are associated with the spaces between multi-adjacent wheels and the frequencies resulting from the train speeds. Random vibrations are functions of forces associated with the running vehicle. They usually arise from the weight of the vehicle and the impact load at the wheel/rail interface, and then transfer into the sub-foundation (Kouroussis et al., 2014). The weight of the vehicle is related to the number of passengers. The impact load corresponds to the speed at which the vehicle runs, which results in different frequencies. Therefore, it is imperative to simulate the vehicle forces and to execute the train speed on the track in a manner that closely approximates the physical problem.

The vibration characteristics are associated with many factors, such as speed, rail type, sleeper, ballast, subgrade, building foundation, and structure (Ding et al., 2010; Kouroussis et al., 2012). The vibrations of the train power system and rail structure, along with the dynamic interactions of wheel/rail and wheel/rail irregularities, are the main vibration sources for the rail structure (Kouroussis et al., 2014). The average weight of one carriage of a metro train with eight wheels is 38 t; therefore, the weight of one wheel acting on one rail is about 4.75 t. One approach to reduce the computational demand of the large 3D models is to use a 2.5D approach (Bian et al., 2011, 2012; Colaço et al., 2015; Connolly et al., 2015a, 2015b). In this approach, the track is not significantly changed in the longitudinal direction, which allows for the problem to be approximated using a 2D geometry while accounting for 3D loading conditions. In the DEM, it is not necessary to implement the vehicle model. This differs from the approach of the finite element method (FEM), in which a complete or partial train is constructed with enormous particles acting on the railway track. It is useful to calculate the dynamic vibrations generated by the approaching train based on the FEM (Connolly et al., 2015a, 2015b) such that the dynamic vibrations are executed directly on tracks by the specific code in PFC with time histories in the DEM.

The random vibration levels acting on rails are illustrated in Fig. 9.

The random vibration levels have five functions, which are assumed to be trigonometric. To excite the train load on the rails mechanically, the middle values (e.g. the middle load between each of two wheels, as marked in Fig. 9) of each function should be assumed. The load between adjacent carriages resembled an "M-shape" in positive values, which is a "W-shape" in negative values (Ricci et al., 2005). The middle value of the "M-shape" load was assumed as the half the peak value. Therefore, the function F_4 can be determined. Based on the distances between adjacent wheels shown in Table 3 and F_4, the middle values of functions F_2 and F_3 are assumed to be a quarter of the peak value and zero, respectively. The functions of F_1 and F_5 are assumed to have initial and end values of zero, respectively. Therefore, the five trigonometric functions for excitation can be expressed as:

$$\begin{aligned}
F_1 &= F_0\left[-1-\sin\left(2\pi f_1 t-\frac{\pi}{2}\right)\right],\\
F_2 &= \frac{F_0}{4}\left[\sin\left(2\pi f_2 t-\frac{\pi}{2}\right)-7\right],\\
F_3 &= F_0\left[\sin\left(2\pi f_3 t-\frac{\pi}{2}\right)-1\right],\\
F_4 &= \frac{F_0}{2}\left[\sin\left(2\pi f_4 t-\frac{\pi}{2}\right)-3\right],\\
F_5 &= F_0[-1-\cos(2\pi f_1 t)],
\end{aligned} \tag{11}$$

where F_1 is the function of the headstock before the first wheel; F_2 is the function of the distance between adjacent wheels; F_3 is the function of the middle block of carriages; F_4 is the function of pontes of adjacent carriages; F_5 is the function of the tailstock after the last wheel. Here, the value of F_0 is 23 750 N, which is half the weight of one wheel (4.75 t), which is used to obtain the middle values and peak values of the load uniformly. f_1, f_2, f_3, and f_4 are the frequencies of these functions.

It is simple to control the train speed on the tracks by controlling the frequency of each function. The frequency is calculated based on the velocity and distance between adjacent wheels:

$$f_i = \frac{v}{L_i}, \tag{12}$$

where v is the velocity of the metro train and L_i is the distance between adjacent wheels (Table 3).

In the present model, the forces with the values of the dynamic vibrations are directly applied to the rail particles, as verified by Zhang et al. (2016). As a train passes the numerical section, the forces are consistent with the values of the above-mentioned five trigonometric functions with different middle values and frequencies in the time domain.

4.7 Whole model of CS-1

To investigate the stability of the tunnel face supported by the concrete lining, a square model with 78 935 particles was constructed. The model was

Table 3 Distances between adjacent wheels

L_i	Distance (m)
Distance of headstock (L_1)	2.5
Distance of wheels (L_2)	2.0
Distance of bogies in a carriage (L_3)	10.0
Distance of wheels (L_4)	5.0
Distance of wheels (L_5)	2.5

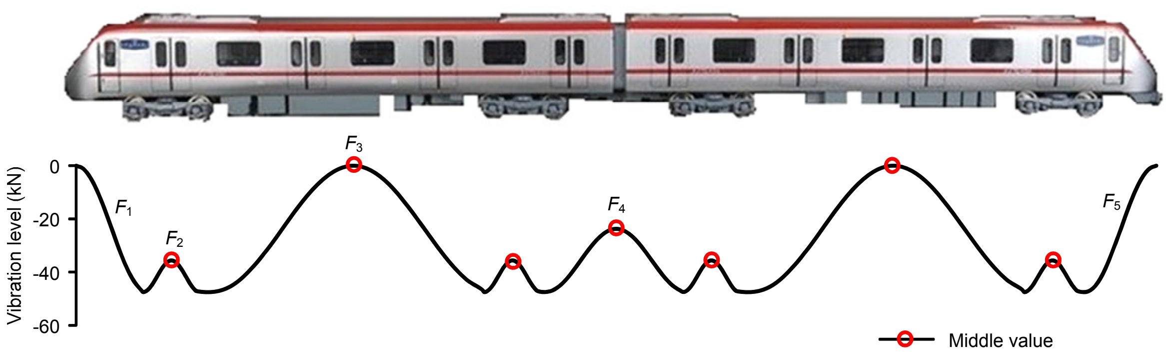

Fig. 9 Illustration of track load with a 2D approach

assembled using uniform particles with the same radius in each stratum, and the micro parameters of each stratum are listed in Table 4.

The size of the model was 15 m×30 m (width×height). The fracture surface of CS-1, for instance, was used as a case to analyze the stability of the concrete lining and the surroundings affected by random train vibrations. Depending on the geology and soil properties, the subsurface soil was divided into several layers, from top to bottom: silty clay, coarse sand (containing some gravel), and coarse sand (containing some cobble), with average water pressure at a depth of 9 m. The rainfall in the Wuhan area started on July 6, 2016, increased its intensity with time and changed to a rainstorm the same day, and lasted for 4 d. This resulted in the flood water level being 10 m higher than the normal water level. Therefore, the water pressures of CS-1 for the cross-river tunnel at the vault were a NWP of 0.294 MPa and a FWP of 0.4 MPa.

To ensure that the proposed model was consistent with engineering practice, the looseness of coarse sand and low strength of mud rock were taken into account. The disturbance of tunnel excavation cannot be neglected due to the discrete surrounding rock, which is a characteristic of the DEM. The vault of the excavation area will be deformed if the lining system is not set up immediately after excavation has finished. To minimize the excavation disturbance zone, the generation of the lining material is implemented immediately after excavation without any calculation steps. The construction stages of the whole model are defined as follows:

Step 1: A square sample with four walls and tens of thousands of particles is generated.

Step 2: Consolidation with the confining stress of the associated water pressure is implemented.

Step 3: The excavation process is activated (Section 4.5).

Step 4: Sleepers are constructed with the expansion command and rails are generated by the ball command.

Step 5: Random vibration levels are produced on the rail.

Note that during the excavation process, although the water pressure is already taken into consideration, because of the highly cohesive bonding and low permeability of the concrete lining, water infiltration is not considered. The model of CS-1 shown in Fig. 10 illustrates the simulation process for step 4.

5 Numerical simulation results

To evaluate the influence of the random vibration level induced by metro train operation under NWP and FWP on the concrete lining and the surroundings, different speeds of the metro train were simulated. In general, the speed of the train is usually restricted to the range from 40 km/h to 100 km/h. Thus, the speeds that were considered were 40, 60, 80, and 100 km/h. Before proceeding to the enormous task of train-speed analysis, the most significant step is to verify the train load that acts on the rails.

5.1 Verification of random vibration level

Before starting the calculation, the basic equations for random vibration levels should be written to

Table 4 Micro-macro parameters in the metro tunnel model

Item	Diameter (m)	Density (kg/m^3)	Normal stiffness (N/m)	Shear stiffness (N/m)	Friction coefficient	Normal strength of parallel bond (Pa)	Shear strength of parallel bond (Pa)	Normal stiffness of parallel bond (N/m)	Shear stiffness of parallel bond (N/m)	Parallel bond radius multiplier
Silty clay	0.06–0.10	1700	2.17×10^6	2.17×10^6	0.185	–	–	–	–	–
Coarse sand (C)	0.06–0.10	2050	3.54×10^7	3.54×10^7	0.90	–	–	–	–	–
Coarse sand (D)	0.06–0.10	2110	3.80×10^7	3.80×10^7	0.84	–	–	–	–	–
Sleeper	0.012	2180	1×10^7	1×10^7	0.5	5×10^9	5×10^9	1×10^9	1×10^9	1
Track	0.10	2630	5.2×10^{10}	5.2×10^{10}	0.0	–	–	–	–	–
Concrete lining	0.009	2180	9×10^8	9×10^8	1.98	7.1×10^9	7.1×10^9	9×10^8	9×10^8	1

obtain the dynamic load as a function of time (Cui et al., 2016). The time step was calculated based on the stiffness and mass of the particles in PFC. The function for calculation of one time step is given as (Itasca, 2008)

$$\Delta t = \sqrt{\frac{m}{k}}, \tag{13}$$

where m is the mass of the particle and k is the stiffness of the particle. The calculated time step in this analysis was about 1×10^{-7} to 1×10^{-6} s.

The length of the metro train was determined as the sum of the lengths of one headstock, four middle carriages, and one tailstock. For the case in which two trains are operating, the random vibration levels with train speeds of 40, 60, 80, and 100 km/h measured from the rails are illustrated in Fig. 11.

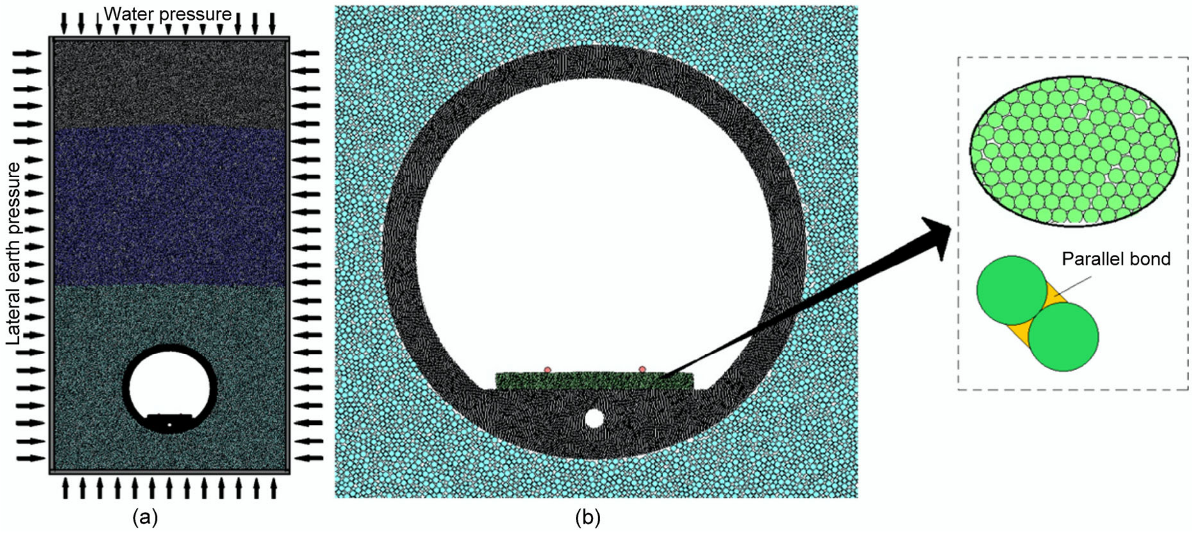

Fig. 10 Illustration of CS-1 of the cross-river tunnel
(a) View of the whole model; (b) Partial illustration of the metro hole with sleeper and rails

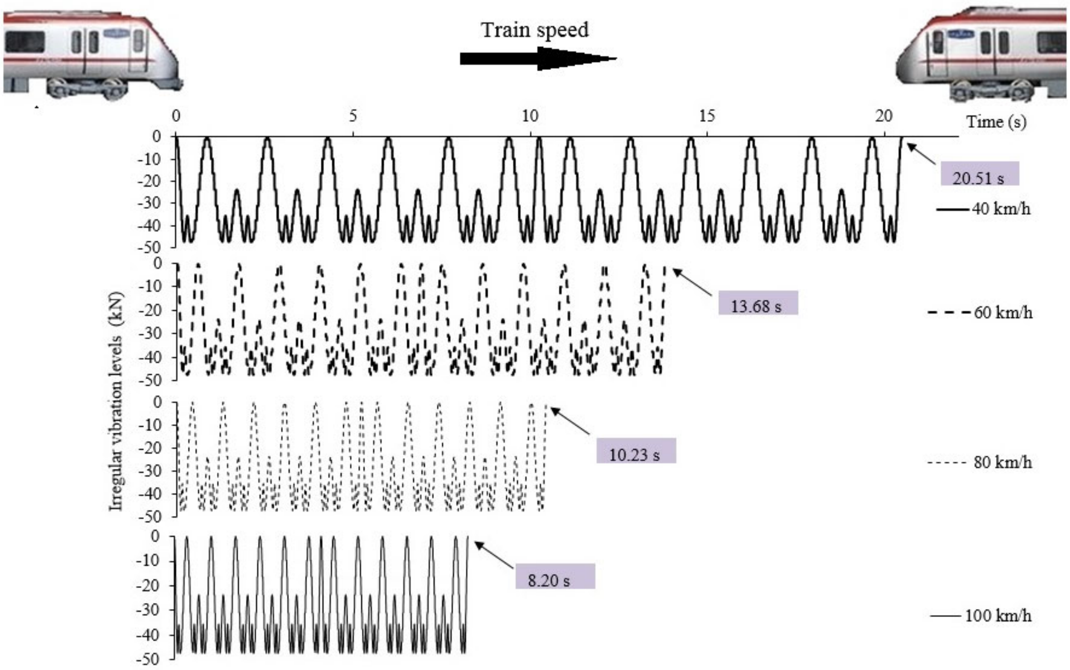

Fig. 11 Random vibration levels with train speeds of 40, 60, 80, and 100 km/h

By comparing Figs. 9 and 11, it can be seen that the vertical load induced by a metro train running with a random vibration level is in good agreement with the values we expected. For two trains to completely pass the cross-section at a velocity of 40 km/h, it will take 20.51 s. As the length of one carriage is 19 m, the total length of two trains is at most 228 m; thus, it will take 20.52 s for the trains to pass. This is consistent with the time measured in the executed procedures.

5.2 Influence of train operation on a cross-river tunnel under NWP

In the numerical model, the surrounding materials and the concrete lining were measured by arranging several measurement points in different positions. The details of the measurement points are shown in Fig. 12. There were 40 measurement points around the cave zone, and the distance d from the outer edge of the lining was enlarged from 0.1 m to 4.0 m. To reveal the disturbance properties of the random vibration level induced by train operation, the horizontal accelerations, vertical accelerations, and radial displacements of the surrounding materials and the concrete lining were taken into account in the present study.

To obtain the horizontal and vertical accelerations, particle velocities at the measurement points were tracked in time domain. While the train was operating, the path-different velocities of these particles could be tracked and written into a text with the corresponding time nodes. The accelerations could be calculated as the ratio of the velocity change and the corresponding time difference, expressed as

$$a_t = \frac{v_{t+\Delta\delta} - v_t}{\Delta\delta}, \tag{14}$$

where v_t and $v_{t+\Delta\delta}$ are the velocities of the measured particle at time t and time $t+\Delta\delta$, respectively. $\Delta\delta$, the corresponding time difference of the velocity change, can be expressed by $\Delta\delta=N\Delta t$, where N=100 is the history steps for one data-writing in the present model. Δt is the one time step in Eq. (13). The accelerations of the measured particle were calculated until the end of the train operation. Therefore, accelerations as the analytical parameters can intuitively reflect the influence of the train operation on the surrounding materials and concrete lining. The radial displacement is an accumulated variable which is tracked and accumulated during train operation.

5.2.1 Effects on concrete lining

With the structure of the tunnel lining as the critical carrier and barrier in the transmission of the vibrating load waves, the analysis of the dynamic characteristics of the tunnel is quite important. After the train operates for a long time, the tightness and stability of the whole tunnel will be disturbed by large vibrations induced by the train and natural-strata consolidation. Large vibrations, in other words, are like seismic events, which will lead to structural-overturning damage. Therefore, it is necessary to evaluate the vibration levels in the concrete lining to predict its stability.

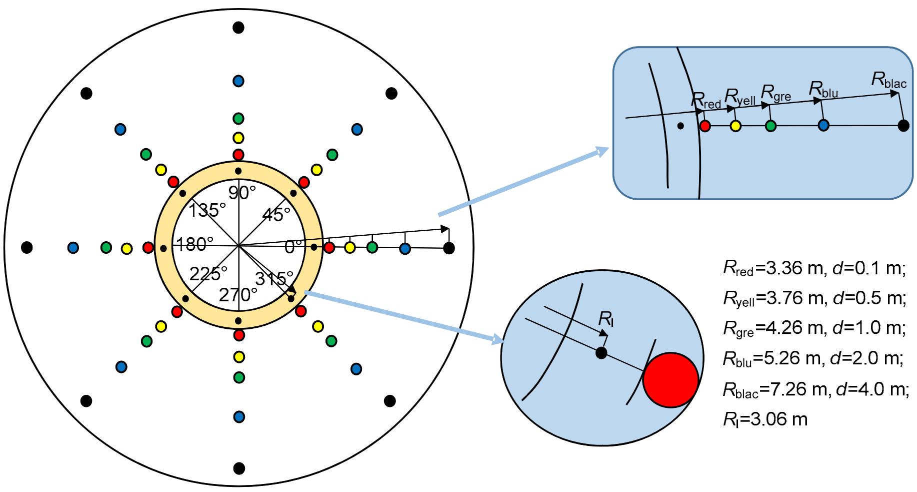

Fig. 12 Illustration of measurement points in the cross-river tunnel (R_l is the radius of the measurement point in concrete lining to the center of the tunnel)

Fig. 13 shows the horizontal and vertical accelerations of particles in the concrete lining at different angles. The entire concrete lining vibrated when the train ran, and the vibration regularities at different angles were roughly consistent with the random vibration levels induced by the train. The vertical accelerations at angles of 0°, 45°, 90°, 135°, and 180° in the upper part of the concrete lining were higher than those at angles of 225°, 270°, and 315° in the lower part of the concrete lining. This is likely to be because vibration waves will be amplified when transmitting from the hypocenter to the transmission path with larger acceleration (Shen et al., 2014).

5.2.2 Effect on the surroundings

Running tunnels have significant effects on the excavation and operation of adjacent tunnels. Chang et al. (2001) reported an event in Taipei, China in which part of a tunnel was disturbed by excavation of an adjacent tunnel. Zhang et al. (2016) constructed a high-speed railway model in which the vibrations induced by train loads were transferred underground for several meters. Thus, to evaluate the influence of metro train loads on the surroundings, it is necessary to consider the acceleration of the surroundings at different distances from the outer edge of the lining.

Vertical acceleration of a particle at each distance was tracked (Fig. 14). The vertical accelerations of particles first increased and then decreased as the distance from the outer edge of the lining increased. The value of the vertical acceleration increased from a distance of 0.1 m to the maximum at a distance of 1.0 m and then decreased. This is likely to be because the kinetic energy generated by the train load is amplified within a finite distance, but then dissipates due to frictional resistance and damping (Zhang et al., 2016). Particles of the surroundings at a distance of 4.0 m had non-ignorable accelerations. This means that the disturbance caused by the metro train operation extended more than 4.0 m from the outer edge of the lining.

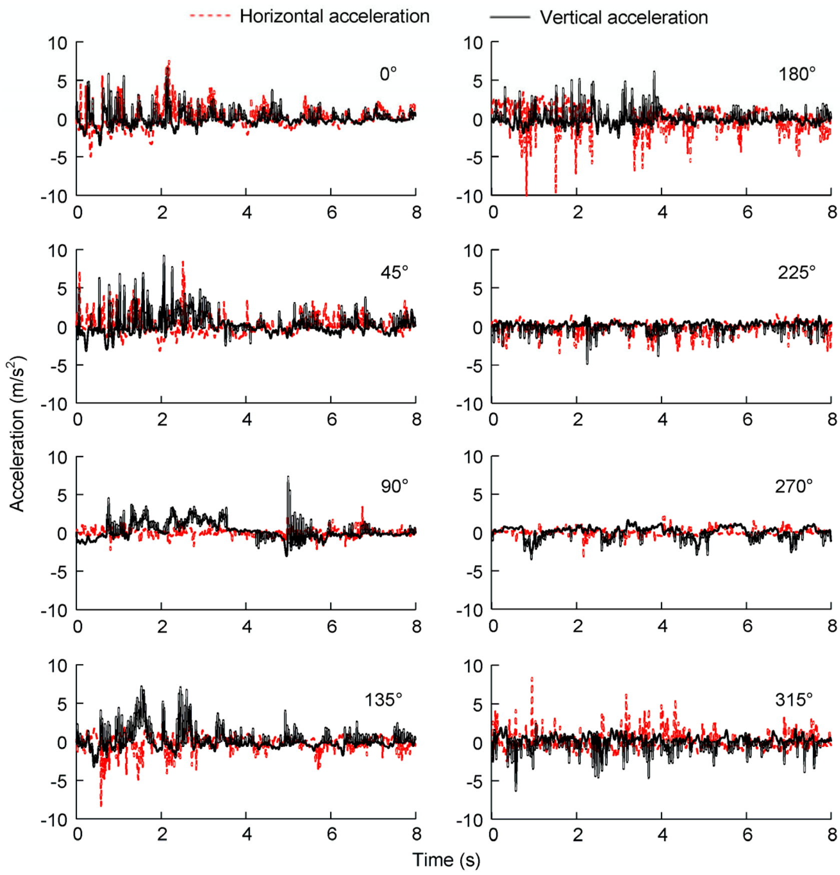

Fig. 13 Illustration of horizontal and vertical accelerations of particles in the concrete lining at different locations with a train speed of 40 km/h under NWP

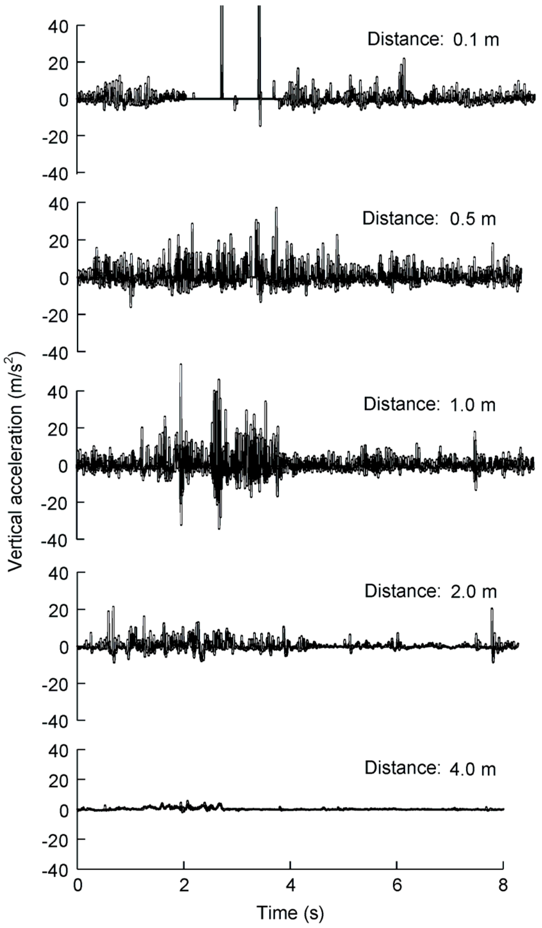

Fig. 14 Vertical accelerations of particles at the vault of the tunnel and the surroundings with a train speed of 40 km/h under NWP

Note that at a distance of 0.1 m between t=2 s and t=4 s, there was very little vertical particle acceleration except for a few specific sharp peaks (Fig. 14). To explain this phenomenon, the vertical stress and vertical displacement of particles around an acceleration-tracked particle at the vault of the tunnel at a distance of 0.1 m were considered. The variation in the time domain is depicted in Fig. 15.

There were two stages in the average vertical stress variation of the monitored particle during the operation of the train between t=2 s and t=7 s: a separation stage and a reassembly stage. In the separation stage between t=2 s and t=4 s, the average stress of the measured particle decreased, as indicated by the negligible contact force chains around the black circle in Fig. 15. The particles were separating from the assembly and dropping down with a steady velocity resulting in zero acceleration. The steady velocity is indicated by the linear increase of the vertical displacement. When the dropping particles contacted the lower particles and the concrete lining, they reassembled. This reassembly stage occurred between t=4 s and t=7 s. In this stage, the contact force increased, as indicated by the force chains in Fig. 15. From the separation stage to the reassembly stage, particles at a distance of 0.1 m were falling continuously. In the process of falling, the vertical acceleration of the measurement point shows several specific and sharp peak values resulting from unavoidable random contacts between adjacent particles.

Xia et al. (2013) studied the influence of adjacent tunnel excavation on an existing tunnel and found that the extent of the rock damage around the existing tunnel increases linearly with the blast load. For cross-river tunnels, each tunnel in two-lane tunnels will be influenced by the vibration level induced by trains operating in the other tunnel. Fig. 16 depicts the vertical acceleration of particles at a distance of 4.0 m from the outer edge of the track lining at different angles. Particles on the right-hand side of the tunnel, shown in the illustration for 0°, had relatively high acceleration at a distance of 4.0 m while the train was running, whereas particles on the left-hand side of the tunnel, shown in the illustration for 180°, had high acceleration during the first 5 s, but then the acceleration decreased to a negligible level. Comparing the illustrations for 45°, 135°, 225°, and 315°, we observe that the duration of the effect of train vibration in the lower part of the tunnel was shorter than that in the upper part. The large acceleration decreased after 3.0 s. Therefore, the effect of an oncoming train on the surroundings in the lower part of the tunnel was smaller than that in the upper part of the tunnel.

5.3 Influence of train operation on a cross-river tunnel under FWP

Rapid increases in the height of the river surface can result in a range of damaging effects, such as dam collapse, water soil erosion, and potential harm to under-river structures. Maximum hourly rainfall cannot be controlled during the flood season. For cross-river tunnels, extreme increases in the height of the river surface will result in increased pore water pressure and bearing pressure around the tunnel. For cross-river tunnels, the flood season should be taken into account in analyses of tunnel stability, especially when metro trains are carrying large numbers of passengers.

In the present model, the flood water level was 10 m higher than the normal water level. The total water pressure of the flood water at the vault of the

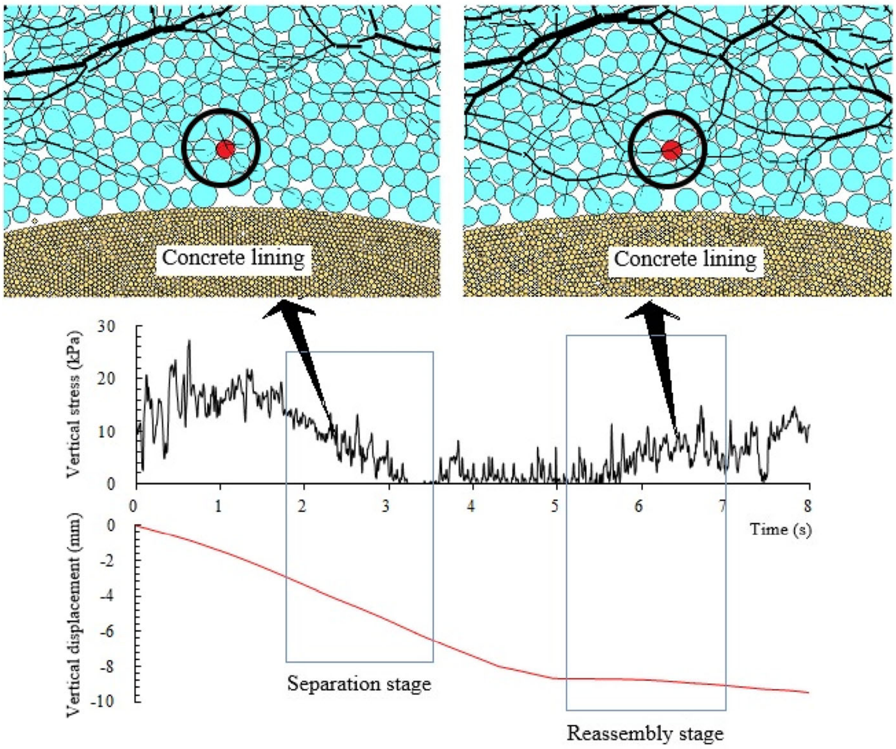

Fig. 15 Vertical average stress and vertical displacement of a particle at the vault of the tunnel at a distance of 0.1 m from the outer edge of the track lining (the particle in the circled area is the acceleration-tracked particle)

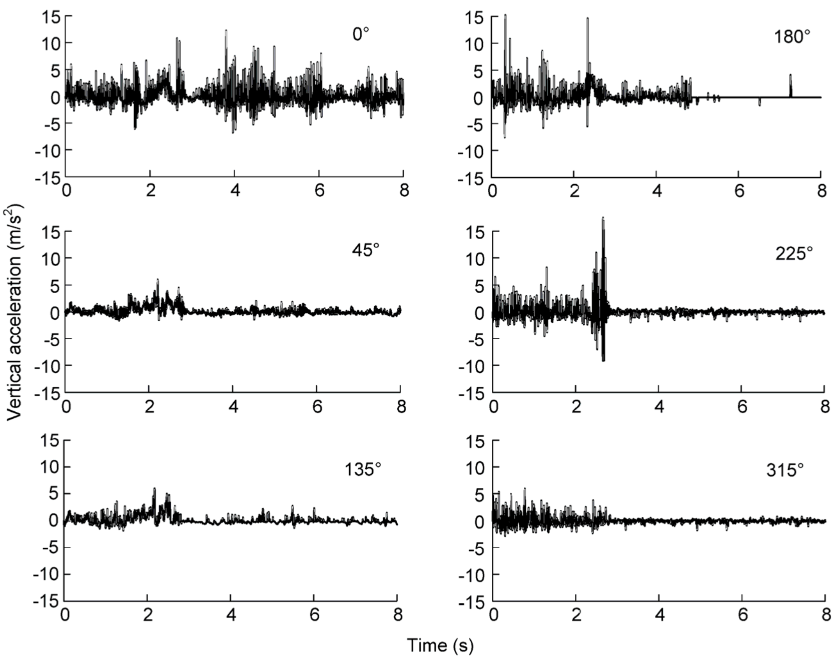

Fig. 16 Vertical accelerations of particles at a distance of 4.0 m from the outer edge of the track lining with a train speed of 40 km/h under NWP

tunnel was up to 400 kPa. Acceleration of particles of the concrete lining and the surroundings were considered when the train speed was 40 km/h.

Particles in the concrete lining under FWP (Fig. 17) exhibited the same acceleration behavior as those under NWP (Fig. 16). However, the values under FWP were much smaller than those under NWP. Particles in the concrete lining in the upper half of the tunnel had higher acceleration than those in the bottom half. By comparing Figs. 13 and 17, we observe that the vertical accelerations of particles above the rail, which had angles in the tunnel ranging from 0° to 180°, were mostly positive; however, those of particles below the rail, which had angles in the tunnel ranging from 225° to 315°, were negative. The sign of these vertical accelerations means that the movements of particles in the concrete lining pointed toward the inside of the tunnel. This is a result of the high confining stress around the tunnel.

The vertical accelerations of particles at different distances from the outer edge of the lining in the surroundings are illustrated in Fig. 18. The accelerations of particles at the vault of the tunnel and the surroundings increased first and then decreased as the distance increased, which is consistent with the results under NWP. The mechanism of the transmission of vibration waves was the same as that under NWP: the vibration waves were amplified. The values of the vertical accelerations, however, were much smaller under FWP (Fig. 18) than under NWP (Fig. 14).

The same phenomenon of specific sharp peaks among zero acceleration values occurred at the distance of 0.1 m. The separating particles dropped down earlier than in the case of NWP based on the zero values, and the separation stage lasted longer. This shows that the deformation of the vault of the tunnel in the surrounding materials under FWP was greater than that under NWP (Section 5.5). The sudden

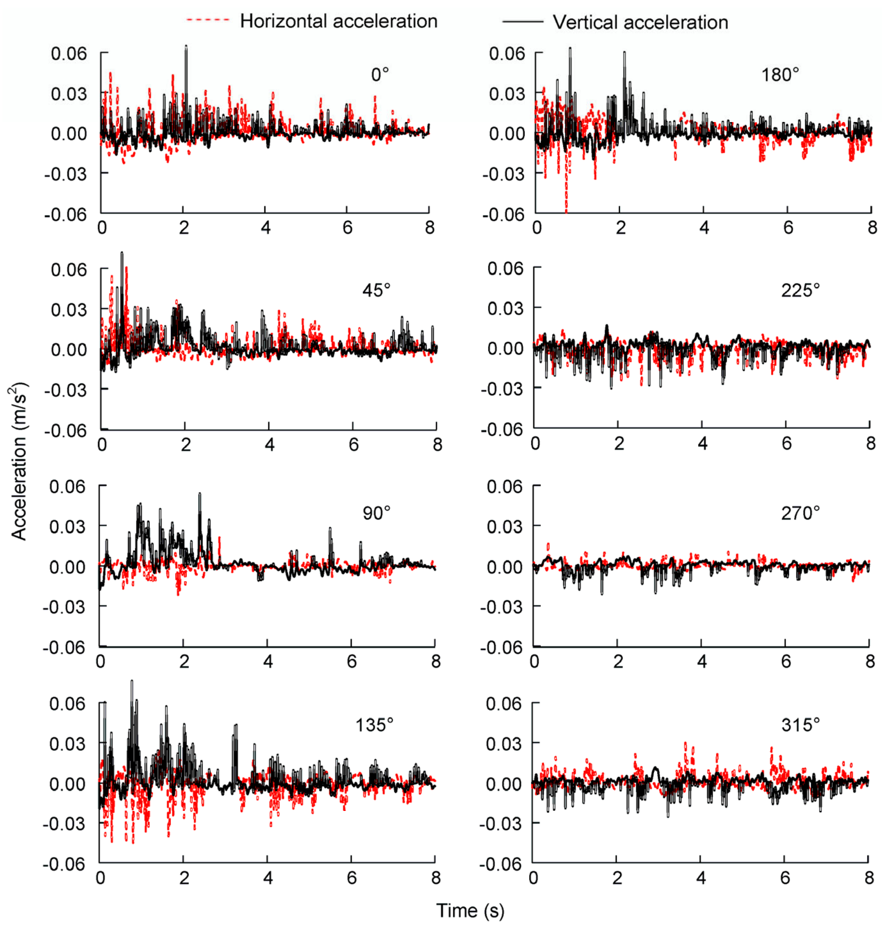

Fig. 17 Illustrations of horizontal and vertical accelerations of particles in the concrete lining at eight different locations with a train speed of 40 km/h under FWP

accelerations of the measurement point occur inevitably due to collisions between adjacent particles during the separation stage.

Note that the vertical acceleration of particles at a distance of 4.0 m from the outer edge of the lining was almost zero (Fig. 18). As a conclusion, the influence of metro train operation on the concrete lining and the surroundings under FWP was lower than that under NWP. In other words, the designation of the buried depth of a cross-river tunnel should be deeper when technology and the in situ strata allow a greater depth to be obtained. Moreover, the strength and stiffness of the concrete lining should be more stable at greater depth.

5.4 Influence of train speed on the tracks and surroundings

With the improvement of technology, train speeds are increasing. Higher speed requires higher equivalent stiffness of the rail foundations. Trains running at high speeds induce important amplifications in the vibration levels of the railway track. Unlike traditional low-speed rail transportation, the impact of the load inflicted by high-speed trains on the track and foundations at different depths will increase significantly as train speed increases (Zhang et al., 2016). Due to Newton's second law, in the DEM, the velocity and acceleration of particles should be considered, as they are associated with the settlement and displacement of the tracks. Therefore, for a cross-river tunnel, it is necessary to examine the impact of train speed on the characteristics of the tracks and the surroundings during operation.

Fig. 19 shows vertical accelerations of the metro track as a function of time, induced by different train velocities. The accelerations were consistent with the random vibration levels induced by the running train. When the train speed increased, vertical acceleration

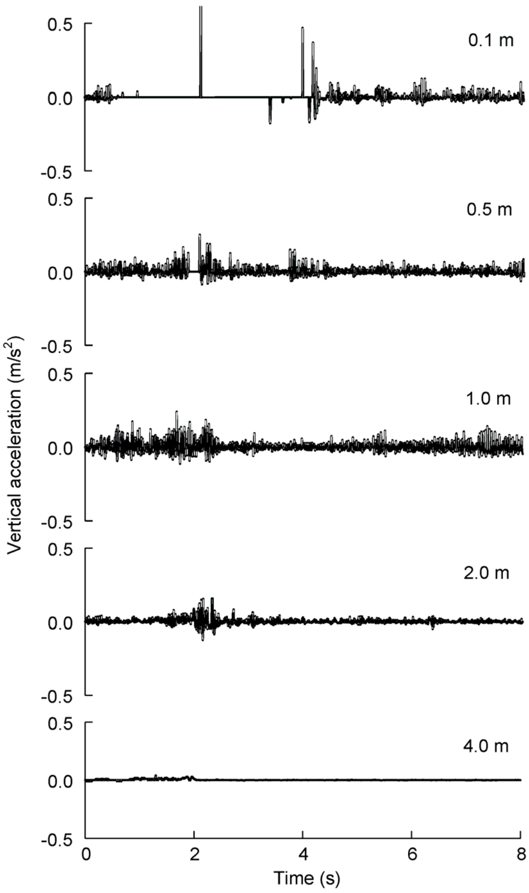

Fig. 18 Vertical accelerations of particles at the vault of the tunnel and at different distances from the outer edge of the track lining with a train speed of 40 km/h under FWP

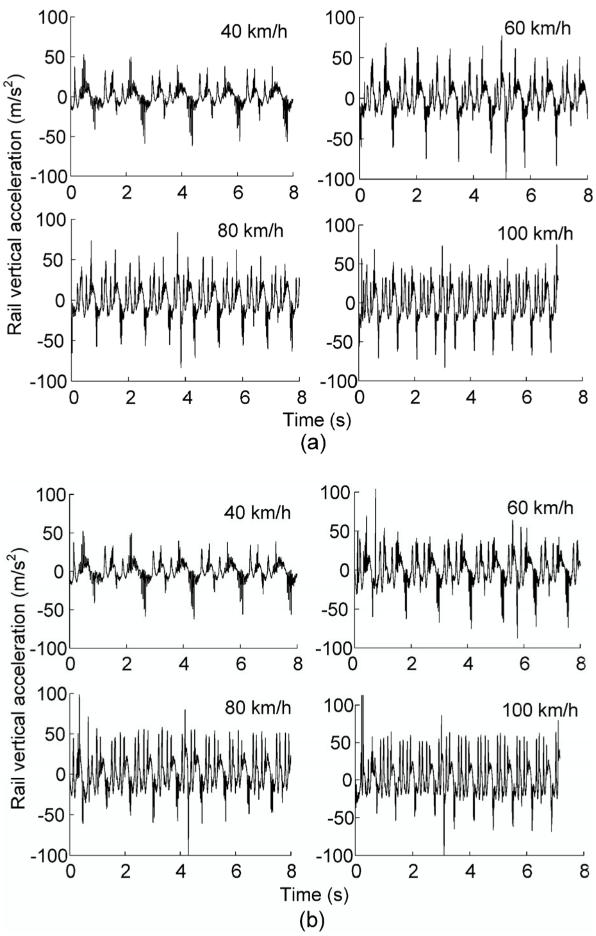

Fig. 19 Rail vertical accelerations induced by different train speeds under NWP (a) and FWP (b)

of the railway track increased. Combined with Newton's second law, the impact load is closely related to the acceleration of the object. For example, the peak value of the vertical acceleration induced by a train speed of 40 km/h under NWP was 50 m/s^2. This is an enormous value, which is equivalent to almost five trains coming across the cross section simultaneously, and may lead to severe deterioration of the railway track and concrete lining. The variation in vertical acceleration with different frequencies is illustrated in Fig. 20.

The vertical acceleration of the tracks increased as train speed increased at the same frequency. A higher load frequency led to higher vertical acceleration. As for the influence of water pressure, a train running under FWP had a greater effect on the rail; in this case, vertical acceleration was greater under NWP than under FWP.

5.5 Influence of train operation on radial displacement

Predicting the settlement of the surroundings around a tunnel has gradually become an important research issue. Radial displacements of the lining and particles around the tunnel under NWP and FWP were tracked (Itasca, 2008) in this study. The distribution of radial displacements of the foundation and surrounding particles after train operation are illustrated in Fig. 21. The large deformation of the surroundings occurred mostly on the vault of the tunnel where the values of radial displacement of the particles reached 10 to 20 cm. This is attributed to several factors, such as the disturbance caused by the excavation process, the settlement induced by high water pressure, and the random vibration level. By comparing the illustrations for NWP and FWP, we observe that the zone of large deformation was wider under FWP than under NWP at the vault of the tunnel. We conclude that an increase in the water-surface level will result in greater deformation of the surroundings, especially in the upper half of the tunnel.

Radial displacement of the track foundation under different train speeds was considered in our model. All particles in the model, including those in the sleeper, track, and substructure, had different levels of displacement (Fig. 22). Comparing Fig. 21 and the details of the track foundation illustrated in Fig. 22, we observe that with increasing train speed, the radial displacements of particles in the track foundation decreased and the disturbance zone induced by metro train operation decreased, as illustrated in Fig. 22 by radial displacements marked by different colors in the surroundings under the tracks. However, vertical acceleration increased when train speed increased.

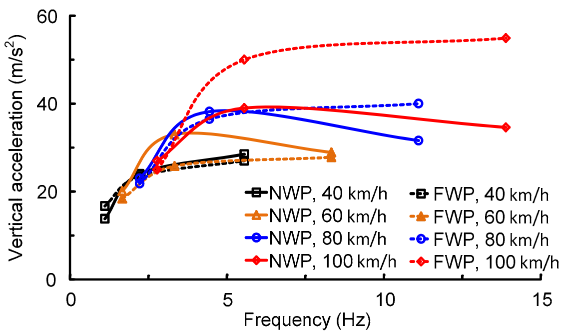

Fig. 20 Illustration of vertical acceleration of tracks with different frequencies under NWP and FWP

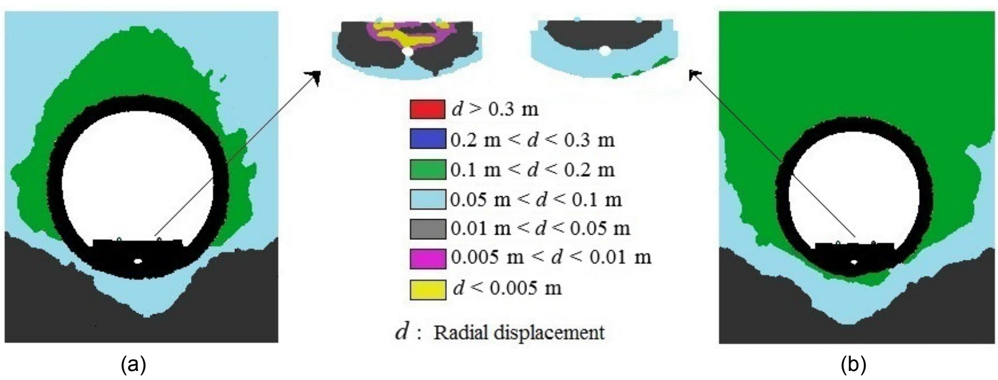

Fig. 21 Radial displacement of particles around the tunnel in this model with a train speed of 40 km/h under NWP (a) and FWP (b)

Note: for interpretation of the references to color in this figure legend, the reader is referred to the web version of this article

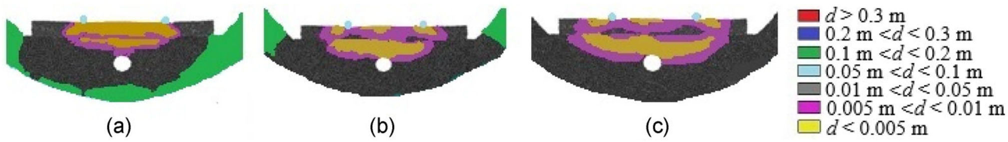

Fig. 22 Radial displacement of the track foundation under FWP after continuous operation of two trains
(a) 60 km/h; (b) 80 km/h; (c) 100 km/h. Note: for interpretation of the references to color in this figure legend, the reader is referred to the web version of this article

6 Conclusions

To investigate the influence of metro train operation on the cross-river tunnel of the Wuhan Metro Line 2 under flood water levels following a recent flood disaster, a large-scale underwater tunnel model with random vibration levels induced by a running train is proposed and implemented with PFC software. In the model, accelerations in the horizontal and vertical paths of the track, the concrete lining, and the surroundings of the tunnel under different train speeds are taken into account. The radial displacement of particles is also considered. Due to the complicated underground geology around the tunnel, the model is simplified and attempts to reveal the mechanics of the tunnel under different water pressures and train speeds. The following conclusions can be drawn:

1. Particles located in the upper half of the tunnel have larger accelerations than those located below the track in the concrete lining, especially those at angles of 45°, 90°, and 135°.

2. Vibration waves are amplified within a finite distance from the outer edge of the lining and then weaken to zero as the distance increases. In our model, the finite distance for the largest vibration level is about 1.0 m, regardless of whether the model is under NWP or FWP.

3. Acceleration levels in the concrete lining and the surroundings are much lower under FWP than under NWP. This means that a metro train operating under higher water pressure (or deeper tunnel construction) will be safer, but will require a higher level of designation and more advanced technology.

4. Higher water pressure leads to larger deformation of the surroundings, concentrated on the upper half of the tunnel. With increasing train speed, accelerations of particles in the track and the substructure increase, resulting in lower radial displacement. The relationship between the frequency of the random vibration level and the vertical acceleration of the track is nonlinear.

Although the simple model proposed cannot completely simulate the in situ situation, it is helpful for the assessment of the safety and stability of the cross-river tunnel during the rainy season. The study of cross-river tunnels, as a main transportation artery in major cities, requires further attention. The DEM has unique advantages for simulating the large deformation of discrete particles. A large amount of work remains to be done, including on the design depth of cross-river tunnels to obtain more desirable stability, and on the influence of adjacent metro operations on the stability of existing tunnels.

References

Abul-Husn NS, Sutak M, Milne B, et al., 2013. Measurement of building foundation and groundborne vibrations due to surface trains and subways. *Engineering Structures*, 53(1): 5-14.
https://doi.org/10.1016/j.engstruct.2013.03.038

Aldea CM, Shah SP, Karr A, 1999. Permeability of cracked concrete. *Materials and Structures*, 32(5):370-376.
https://doi.org/10.1007/BF02479629

Bian XC, Chao C, Jin WF, et al., 2011. A 2.5D finite element approach for predicting ground vibrations generated by vertical track irregularities. *Journal of Zhejiang University-SCIENCE A (Applied Physics & Engineering)*, 12(12): 885-894.
https://doi.org/10.1631/jzus.A11GT012

Bian XC, Jin WF, Jiang HG, 2012. Ground-borne vibrations due to dynamic loadings from moving trains in subway tunnels. *Journal of Zhejiang University-SCIENCE A (Applied Physics & Engineering)*, 13(11):870-876.
https://doi.org/10.1631/jzus.A12ISGT5

Chang CT, Sun CW, Duan SW, et al., 2001. Response of a Taipei rapid transit system (TRTS) tunnel to adjacent excavation. *Tunnelling & Underground Space Technology*, 16(3):151-158.
https://doi.org/10.1016/S0886-7798(01)00049-9

Colaço A, Costa PA, Connolly DP, 2015. The influence of train properties on railway ground vibrations. *Structure & Infrastructure Engineering*, 12(5):1-18.

https://doi.org/10.1080/15732479.2015.1025291

Connolly DP, Kouroussis G, Laghrouche O, et al., 2015a. Benchmarking railway vibrations–track, vehicle, ground and building effects. *Construction & Building Materials*, 92:64-81.
https://doi.org/10.1016/j.conbuildmat.2014.07.042

Connolly DP, Costa PA, Kouroussis G, et al., 2015b. Large scale international testing of railway ground vibrations across Europe. *Soil Dynamics & Earthquake Engineering*, 71:1-12.
https://doi.org/10.1016/j.soildyn.2015.01.001

Cui Y, Nouri A, Chan D, et al., 2016. A new approach to DEM simulation of sand production. *Journal of Petroleum Science & Engineering*, 147:56-67.
https://doi.org/10.1016/j.petrol.2016.05.007

Ding DY, Gupta S, Liu WN, et al., 2010. Prediction of vibrations induced by trains on line 8 of Beijing metro. *Journal of Zhejiang University-SCIENCE A (Applied Physics & Engineering)*, 11(4):280-293.
https://doi.org/10.1631/jzus.A0900304

Dinis Ferreira PA, 2010. Modeling and Prediction of the Dynamic Behavior of Railway Infrastructures at Very High Speeds. PhD Thesis, Technical University of Lisbon, Lisbon, Portugal.

Fryba L, 1999. Vibration of Solids and Structures under Moving Loads, 3rd Edition. Thomas Telford, London, UK.

Gao WL, Yang MS, Zhao BM, 2012. Seismic response analysis of large span tunnel across the river under earthquake. *Highway*, 5:344-349 (in Chinese).

Gu X, Lu L, Qian J, 2017. Discrete element modeling of the effect of particle size distribution on the small strain stiffness of granular soils. *Particuology*, 32:21-29.
https://doi.org/10.1016/j.partic.2016.08.002

Itasca (Itasca Consulting Group, Inc.), 2008. PFC Particle FOW Code, Version 4.0. Itasca, Minneapolis, USA.

Ji F, Lu J, Shi Y, et al., 2013. Mechanical response of surrounding rock of tunnels constructed with the TBM and drill-blasting method. *Natural Hazards*, 66(2):545-556.
https://doi.org/10.1007/s11069-012-0500-2

Kouroussis G, 2013. Experimental study of ground vibrations induced by Brussels IC/IR trains in their neighbourhood. *Mechanics & Industry*, 14(2):99-105.
https://doi.org/10.1051/meca/2013059

Kouroussis G, Conti C, Verlinden O, 2012. Efficiency of resilient wheels on the alleviation of railway ground vibrations. *Proceedings of the Institution of Mechanical Engineers, Part F: Journal of Rail and Rapid Transit*, 226(4):381-396.
https://doi.org/10.1177/0954409711429210

Kouroussis G, Connolly DP, Verlinden O, 2014. Railway-induced ground vibrations–a review of vehicle effects. *International Journal of Rail Transportation*, 2(2):69-110.
https://doi.org/10.1080/23248378.2014.897791

Ling XZ, Chen SJ, Zhu ZY, et al., 2010. Field monitoring on the train-induced vibration response of track structure in the Beiluhe permafrost region along Qinghai-Tibet railway in China. *Cold Regions Science & Technology*, 60(1): 75-83.
https://doi.org/10.1016/j.coldregions.2009.08.005

Liu Z, Koyi H, 2013. Kinematics and internal deformation of granular slopes: insights from discrete element modeling. *Landslides*, 10(2):139-160.
https://doi.org/10.1007/s10346-012-0318-8

Lu JF, Zhang CW, Jian P, 2017. Meso-structure parameters of discrete element method of sand pebble surrounding rock particles in different dense degrees. Proceedings of the 7th International Conference on Discrete Element Methods, p.871-879.
https://doi.org/10.1007/978-981-10-1926-5_91

Min FL, Zhu W, Han XR, et al., 2010. The effect of clay content on filter cake formation in highly permeable gravel. *Geoshanghai International Conference*, 204:210-215.
https://doi.org/10.1061/41105(378)29

Min FL, Zhu W, Lin C, et al., 2015. Opening the excavation chamber of the large-diameter size slurry shield: a case study in Nanjing Yangtze River Tunnel in China. *Tunnelling and Underground Space Technology*, 46:18-27.
https://doi.org/10.1016/j.tust.2014.10.002

Nielsen J, Lundén R, Johansson A, et al., 2003. Train-track interaction and mechanisms of irregular wear on wheel and rail surfaces. *Vehicle System Dynamics*, 40(1-3):3-54.
https://doi.org/10.1076/vesd.40.1.3.15874

Picandet V, Khelidj A, Bellegou H, 2009. Crack effects on gas and water permeability of concretes. *Cement & Concrete Research*, 39(6):537-547.
https://doi.org/10.1016/j.cemconres.2009.03.009

Potyondy DO, Cundall PA, 2004. A bonded-particle model for rock. *International Journal of Rock Mechanics & Mining Sciences*, 41(8):1329-1364.
https://doi.org/10.1016/j.ijrmms.2004.09.011

Ricci L, Nguyen VH, Sab K, et al., 2005. Dynamic behavior of ballasted railway tracks: a discrete/continuous approach. *Computers and Structures*, 83(28-30):2282-2292.
https://doi.org/10.1016/j.compstruc.2005.03.035

Shen Y, Gao B, Yang X, et al., 2014. Seismic damage mechanism and dynamic deformation characteristic analysis of mountain tunnel after Wenchuan earthquake. *Engineering Geology*, 180:85-98.
https://doi.org/10.1016/j.enggeo.2014.07.017

Voit K, Zimmermann T, 2015. Characteristics of selected concrete with tunnel excavation material. *Construction & Building Materials*, 101:217-226.
https://doi.org/10.1016/j.conbuildmat.2015.10.016

Wang J, Gutierrez M, 2010. Discrete element simulations of direct shear specimen scale effects. *Géotechnique*, 60(5): 395-409.
https://doi.org/10.1680/geot.2010.60.5.395

Wu K, Pizette P, Becquart F, et al., 2017. Experimental and numerical study of cylindrical triaxial test on mono-sized glass beads under quasi-static loading condition.

Advanced Powder Technology, 28(1):155-166. https://doi.org/10.1016/j.apt.2016.09.006

Xia X, Li HB, Li JC, et al., 2013. A case study on rock damage prediction and control method for underground tunnels subjected to adjacent excavation blasting. *Tunnelling & Underground Space Technology*, 35:1-7. https://doi.org/10.1016/j.tust.2012.11.010

Xiong C, 2014. Technical characteristics and innovation of the cross-Yangtze river tunnel of Wuhan subway line No. 2. *Railway Survey and Design*, 3:1-7 (in Chinese).

Zhai W, Wei K, Song X, et al., 2015. Experimental investigation into ground vibrations induced by very high speed trains on a non-ballasted track. *Soil Dynamics & Earthquake Engineering*, 72:24-36. https://doi.org/10.1016/j.soildyn.2015.02.002

Zhang S, Xia Y, Ma G, et al., 2013. Reconnaissance and construction key issues for the cross-river tunnel of Wuhan subway line No. 2. *Chinese Journal of Underground Space and Engineering*, 9(4):914-918 (in Chinese).

Zhang Z, Zhang X, Qiu H, et al., 2016. Dynamic characteristics of track-ballast-silty clay with irregular vibration levels generated by high-speed train based on DEM. *Construction & Building Materials*, 125:564-573. https://doi.org/10.1016/j.conbuildmat.2016.08.079

Zhou Y, Su K, Wu H, 2015. Hydro-mechanical interaction analysis of high pressure hydraulic tunnel. *Tunnelling & Underground Space Technology*, 47:28-34. https://doi.org/10.1016/j.tust.2014.12.004

中文概要

题　目： 汛期地铁行车荷载作用下越江隧道离散元分析

目　的： 揭示汛期及常水位条件下地铁随机振动荷载作用下越江隧道管片及周边岩土体的动力响应及变形机制。

创新点： 建立越江地铁隧道二维离散元模型，并采用随机振动荷载模拟地铁行车荷载，揭示汛期和常水位条件下地铁行车荷载对越江隧道稳定性的影响。

方　法： 采用离散元方法进行数值仿真。1. 基于室内三轴试验和离散元数值拟合得到土层的各细观参数；2. 采用不同接触模型对隧道内钢轨、轨枕、管片以及周边岩土体进行建模；3. 将地铁随机振动荷载施加在钢轨上，对管片及周边岩土体不同区域内颗粒的受力及变形进行监测并分析。

结　论： 1. 位于隧道上半部分的周边岩土体颗粒振动偏大；2. 随着距离的增大，振动波在周边岩土体内先放大后减小；3. 汛期水位条件下地铁行车荷载对管片和周边岩土体的振动影响较小，但是对隧道变形影响较大。

关键词： 离散元方法；越江地铁隧道；水压力；地铁行车荷载